Applied Catalysis B: Environmental 184 (2016) 191–200

Contents lists available at ScienceDirect

Applied Catalysis B: Environmental

journal homepage: www.elsevier.com/locate/apcatb

From the fluorescent lamp-induced bactericidal performance of sputtered Ag/TiO_2 films to re-explore the photocatalytic mechanism

Dong-Hau Kuo[a,*], Wei-Ting Hsu[a], Yi-Yuan Yang[b]

[a] Department of Materials Science and Engineering, National Taiwan University of Science and Technology, Taipei 10607, Taiwan
[b] School of Medical Laboratory Science and Biotechnology, Taipei Medical University, Taipei 11031, Taiwan

ARTICLE INFO

Article history:
Received 16 April 2015
Received in revised form 20 July 2015
Accepted 21 November 2015
Available online 30 November 2015

Keywords:
Photocatalysis
Composite catalyst film
Antibactericide
TiO_2
Ag nano particle

ABSTRACT

Ag/TiO_2 composite films with the different Ag contents of 1, 3, and 5 vol.% were deposited at 25, 200, and 400 °C on glass substrates by radio frequency sputtering with a single cermet target formed by hot pressing the Ag nanoparticle-decorated TiO_2 nanopowder at 900 °C in argon atmosphere for 30 min, followed by annealing in air and the reduction under vacuum heating or by $NaBH_4$. All the TiO_2 films were analyzed by X-ray diffraction technique to have an amorphous structure. High deposition and annealing temperatures all led to Ag aggregation in Ag/TiO_2. Photodegradation of acid black 1 dye was used as the screen test to evaluate the photocatalytic ability of Ag/TiO_2 films, before the antibacterial test was preceded. The antibacterial ability on *Escherichia coli* was also evaluated. The 25 °C-deposited 3% Ag/TiO_2 films of 80 nm in thickness had the best performance in optical transmittance above 70% and killing the *E. coli*. The mechanism for the fluorescent lamp-induced bactericide of the 3% Ag/TiO_2 film is proposed. The amorphous 3% Ag/TiO_2 film had larger band gap of 3.67 eV than the annealed ones and is expected not to be excited by the fluorescent lamp, but to prolong the lifetime of the thermally induced, not photo-induced, charge carriers in the Ag/TiO_2 by its electric field of the illumination light and the attraction by Ag nanoparticles <8 nm in size. The Ag^+ release mechanism for bactericide is not the major one here after comparing with the tests in the dark.

1. Introduction

TiO_2 is an *n*-type semiconductor photocatalyst with band-gap energy of 3.2 eV. When a photon at equal or higher energy ($\lambda \leq 400$ nm) illuminates on TiO_2, the photon energy can generate the electron–hole pairs inside TiO_2 for the redox reactions. Its applications range from water splitting [1], optoelectronics [2], gas sensing [3], anti-bacteria [4,5], organic photodegradation [6], solar energy conversion [7] etc. To greatly harvest the solar energy and better photochemical reactions, the composite-type TiO_2 photocatalysts have been widely pursued by the combinations of pure, cation- and anion-doped, and co-doped TiO_2 with metals and non-metals [8,9].

Metal-loaded TiO_2 powder has been used to enhance the efficiency of the photocatalytic process by separating the photo-induced charges with the conducting metal as a reservoir [10,11] and by the surface plasma resonance (SPR) of metal nanoparticle [12]. Many metals (Ag, Cu, Co, Fe, Ce, Al, Cr, Nd etc.) have been attached onto TiO_2 to form Ti–O–Ag by absorbing Ag^+ on the hydroxylated TiO_2 surface [13,14]. Ag metal had shown better performance. The presence of Ag deposits on the TiO_2 surface enhanced the photo-oxidation of oxalic acid by a factor of 5 times, because the amount of excited oxygen atoms increased [15]. Additional benefit of adding Ag on TiO_2 is its antibacterial ability.

As TiO_2-based slurry has a disadvantage of separating and removing catalyst particles from solution after photocatalytic reactions, the immobilization of TiO_2 in the form of thin film can be one of the solutions. However, Ag-embedded TiO_2 (Ag/TiO_2) thin film, with much lower specific surface area to the Ag nanoparticle-decorated TiO_2 powder, is expected to have low photocatalytic capability. Ag/TiO_2 composite films have been prepared via sol–gel route [4], photo reduction of Ag under UV irradiation on nanoporous TiO_2 by spin-coating [16,17], and hybrid Ag sputtering/TiO_2 sol–gel routes [18]. The sputter depositions for TiO_2/Ag/TiO_2 stacking with the Ti and Ag targets [19] and with the TiO_2 and Ag targets [20] had been used for Ag/TiO_2 composite films after a heat treatment was conducted to disperse the Ag film into the embedded Ag nanoparticles into TiO_2. All the mentioned processes for Ag/TiO_2 have the problem of Ag aggregation under process heating or even squeezing out to the surface of TiO_2 film. The Ag aggregates with a size larger than 10 nm showed the SPR enhancement and increased the visible light absorption of Ag/TiO_2

* Corresponding author. Fax: +886 2 27303291.
E-mail address: dhkuo@mail.ntust.edu.tw (D.-H. Kuo).

http://dx.doi.org/10.1016/j.apcatb.2015.11.032
0926-3373/

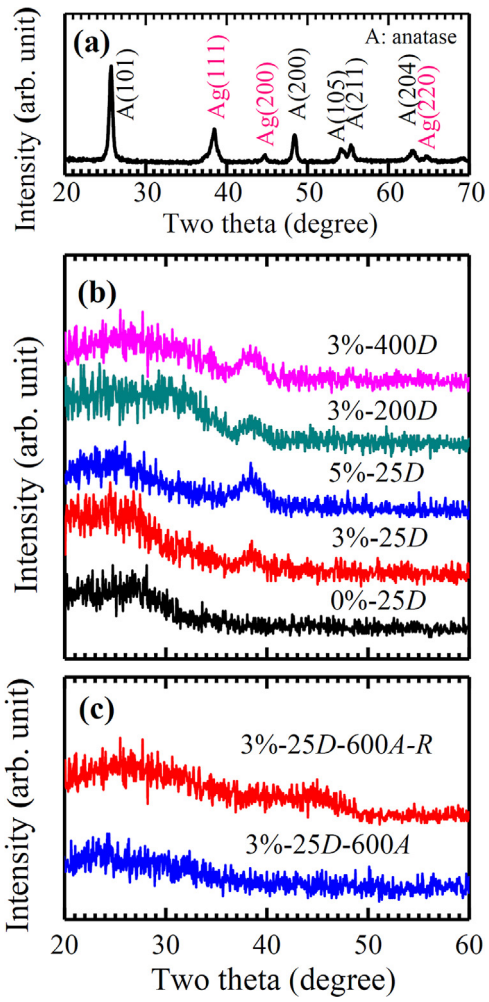

Fig. 1. XRD diffraction analyses of (a) 3% Ag/TiO_2 powder before hot pressing for target, (b) Ag/TiO_2 films prepared with targets of different Ag contents and at different growth temperatures, and (c) the 25 °C-deposited 3% Ag/TiO_2 films after annealing at 600 °C in air (A) followed with and without the reduction by $NaBH_4$ (R).

film to harvest the visible light photocatalysis. On the contrast, the visible light absorption leads to the second problem of Ag/TiO_2 film for its low visible light transparency.

In this work, Ag/TiO_2 films were sputtered with 1–5 vol.% Ag/TiO_2 cermet targets, which were prepared by hot pressing Ag/TiO_2 powders with the attached Ag nanoparticles formed by the Ag^{1+} reduction with an agent of $NaBH_4$. Our Ag nanoparticle-attached TiO_2 targets had Ag particles separated and blocked by TiO_2 during deposition to avoid (1) the problem of Ag aggregation from the layer-by-layer deposition with its aggregate size close to the Ag film thickness and (2) the co-sputtering problem in controlling the extremely low Ag input flux together with the TiO_2 flux. The behaviors of our Ag/TiO_2 films on photocatalysis, optical transparency, and antibacterial activity were evaluated.

2. Experimental

2.1. Ag/TiO_2 composite nanoparticles

Anatase TiO_2 nanoparticles of 40–50 nm in size were purchased from Advanced Ceramics Nanotech Co., in Taiwan. The required $AgNO_3$ contents for 1, 3, and 5 vol.% Ag/TiO_2 were added into the TiO_2 suspensions, which were stirred for 2 h. The required $NaBH_4$ for reduction was dissolved in a 10 ml aqueous solution. The Ag-reduced solution was dried by a vacuum evaporator followed by grinding into composite powder.

2.2. Ag/TiO_2 composite films

The 2-inch sputtering targets of Ag/TiO_2 with different Ag contents were prepared by hot pressing the composite powders. The Ag/TiO_2 films were deposited at substrate temperatures of 25 °C, 200 °C, and 400 °C on soda lime glass substrates of 20 × 20 × 1 mm in size by radio frequency (r.f.) magnetron sputtering at 80 W for 1 h under the argon atmosphere. The pure TiO_2 film was prepared with the same procedure for the comparison purpose.

Some Ag/TiO_2 films were undergone the annealing at 400, 500, and 600 °C for 1 h in air or in nitrogen. Some air-annealed (symbolized as A) Ag/TiO_2 films were immersed in a $NaBH_4$ solution for a reduction reaction (symbolized as *R*) to form pure Ag.

2.3. Characterizations

A Bruker D8 Discover SSS X-ray diffractometer operating with Cu-Kα radiation (λ = 0.15406 nm) at 40 kV and 40 mA was used to determine the changes in crystal structure. The grazing incidence operating mode was used with an incidence angle of 1° and the sampled step size was 0.01° within 2θ = 20–60°. Field-emission scanning electron microscopy (FE-SEM, JSM 6500F, JEOL, Tokyo, Japan) was used to observe surface morphology. Field-emission transmission electron microscopy (FE-TEM, Tecnai F20 G2, Philips, Netherlands) was used to analyze the microstructure. The surfaces were further visualized by an atomic force microscope (AFM, Dimension Icon, Bruker). Dual beam focused ion beam SEM (Quanta 3D FEG, FEI, Oregon, USA) was used to prepare the cross-sectional specimen for FE-TEM. The Optical transmittance of our films was recorded in the wavelength range of 300–800 nm using a Jasco V-670 UV–visible-Near IR Spectrophotometer.

2.4. Photodegradation of acid black 1 (AB 1) dye

To select the better photocatalysts, the screen test of dye photodegradation is conducted under the illumination of a 450 W Hg–Xe ultraviolet lamp having a distance of 60 cm to the test solution. An infrared filter was inserted in between. For the light irradiation, the Ag/TiO_2 films were dispersed in a 50 ml dye solution of 10 ppm. The photodegradation was monitored by a Jasco V-670 UV–visible-Near IR Spectrophotometer for the absorbance intensity at 615 nm upon the change in the concentration of AB 1 dye after illumination for 80 min.

2.5. Photo cell killing activity

Antibacterial properties of the films were investigated by a standard drop test method in a dark room. *Escherichia coli* (*E. coli*) stains (ER 2738) were cultured in 15 ml sterilized LB broth with constant shaking at 37 °C overnight in a sterilized conical tube. The suspended bacteria were agglomerated by centrifuging at 4000 rpm for 10 min. The cell pellet was re-suspended in sterilized deionized water and diluted. The 1.0 optical density (OD) of 6×10^7 CFU/ml at a wavelength of 600 nm was obtained by comparing 1 ml cell solution with the 1 ml LB broth solution as a background. After the dilution of the 1.0 OD solution with the LB broth, the final cell solution had a concentration of 2×10^5 CFU in each 50 μl solution. Each film coated on glass substrate with a dimension of 20 × 20 mm was kept in dark and loaded with 50 ml cell solution. The 20 W fluorescent lamp (FL20D-10, China Electric MFG. Corp., Taiwan) with the light wavelength between 380–780 nm, which is a common light source for indoor lighting, was continuously illuminated on test samples with the intensity of 680 lm/m^2 and was kept a constant

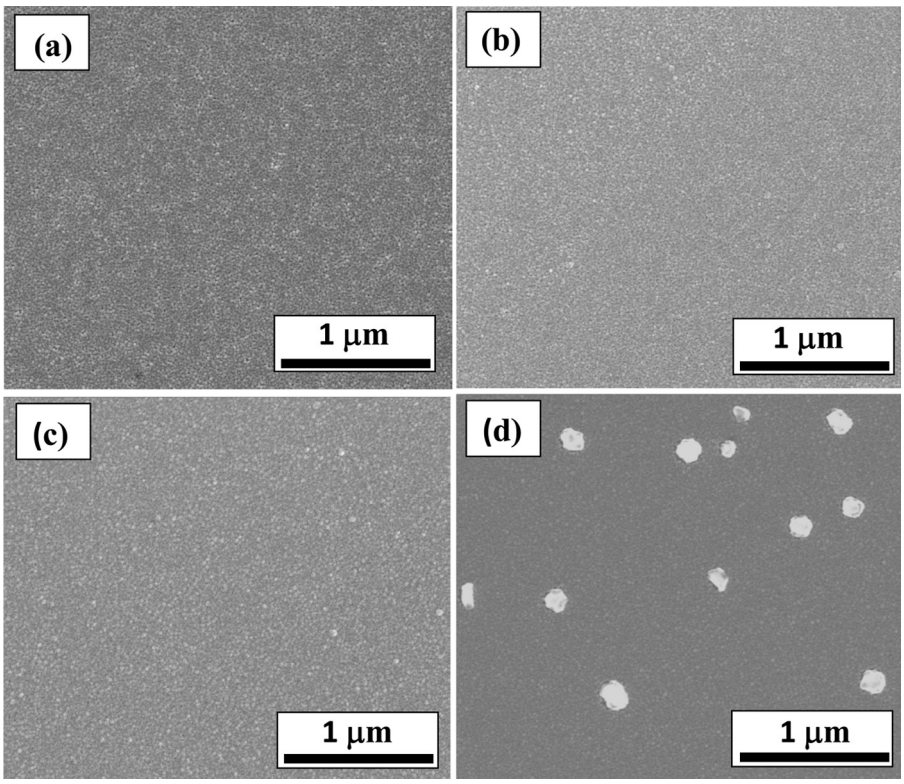

Fig. 2. SEM surface images of the (a) 3% Ag/TiO_2 and (b) 5% Ag/TiO_2 composite films grown at 25 °C and the 3% Ag/TiO_2 films deposited at (c) 200 °C and (d) 400 °C without any post-treatment.

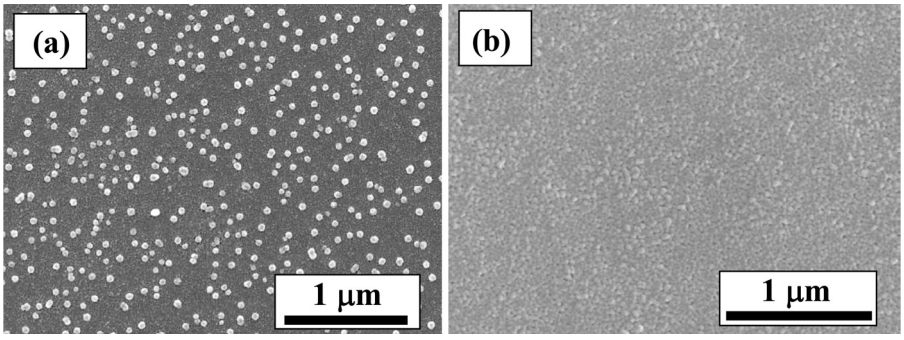

Fig. 3. SEM surface images of the 25 °C-deposited 3% Ag/TiO_2 composite films (a) after 600 °C annealing in pure N_2 and (b) after 600 °C annealing in air and a following vacuum reduction at 400 °C.

distance of 30 cm. The cell solution of 10 μl was collected at regular intervals of 30 and 60 min. The 10 μl solution was for a diluted solution with a factor of 1000. This diluted solution of 50 μl was spread on the LB agar plate and dried, followed by oven drying with the agar face down at 37 °C for 12 h to complete the test. To measure the antibacterial activity in the dark, the experiment was carried out under similar conditions without illumination. The surviving colonies were counted by eye with the help of a magnifying glass and the bacterial survival was calculated according to the following formula (Eq. (1)):

$$\text{Bacterial survival percentage or BS\%} = 100\% \times \frac{(N_{exp})}{(N_{ref})} \quad (1)$$

where N_{exp} is the live number of bacterial cells on coated substrate and N_{ref} is the live number of bacterial cells on the un-coated glass substrate. The bactericide percentage (BC%) is equal to (100%–BS%).

3. Results and discussion

3.1. Characterizations of as-deposited Ag/TiO_2 films at different process conditions

Fig. 1a shows XRD diffraction analyses of 3% Ag/TiO_2 powder before hot pressing for target. From the powder diffraction, the commercially available TiO_2 was well crystallized. Ag nanoparticles after a reduction process also had crystallized well with the diffraction peaks contributed from the (1 1 1), (2 0 0), and (2 2 0) planes. After sputtering at different substrate temperatures, the obtained Ag/TiO_2 films prepared with targets of different Ag contents were analyzed by XRD, as shown in Fig. 1b. There were no observable peaks contributed from TiO_2. The only detected peak at ~38.5° was contributed from Ag. These data indicate that all TiO_2-related films did not have a good crystallinity, even though the film was grown at

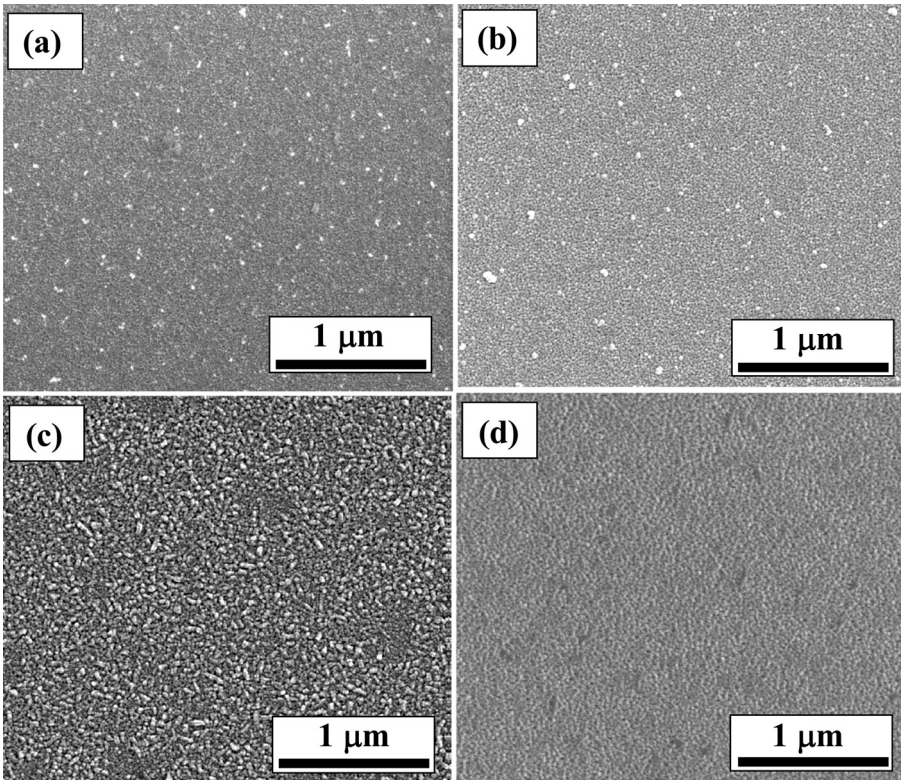

Fig. 4. SEM surface images of the 25 °C-deposited 3% Ag/TiO_2 films after annealing at (a) 400 °C, (b) 500 °C, and (c) 600 °C in air and a following reduction reaction by $NaBH_4$ and (d) SEM image of 25 °C-deposited 3% Ag/TiO_2 film after annealing at 500 °C in air without a reduction reaction for the comparison purpose.

high temperature of 400 °C. As the pure TiO_2 film also displayed an amorphous structure, the difficulty in its crystallization is related to the confinement from the glass substrate.

Fig. 2 shows SEM surface images of the (a) 3% Ag/TiO_2 and (b) 5% Ag/TiO_2 composite films grown at 25 °C and the 3% Ag/TiO_2 films deposited at (c) 200 °C and (d) 400 °C without any post-treatment. The data infer that the 25 °C-deposited TiO_2 films had a dense and smooth microstructure, which had made these images difficult to be observed even under a magnification of ×100,000. Once the growth temperature increased, the 3% Ag/TiO_2 film had the Ag aggregates on the surface (Fig. 2(d)). The Ag aggregates of ~40 nm in size became much observable after the film grew at 400 °C. Any heating for the Ag-containing composite films is not favorable. With the Ag aggregation, there are some instantaneous problems: (1) Ag protrusion and peeling and (2) precipitation leading to the non-uniform Ag distribution with the Ag-depletion zone around Ag aggregates. It looks like the Ag precipitation is not recommended in Ag/TiO_2 composite films. However, Ag nanoparticles have gotten much attention because of its surface plamonic resonance phenomenon.

For the study of the Ag content in TiO_2 for photodegradation, the tests of the 25 °C-deposited Ag/TiO_2 composite films with 0, 1, 3, and 5% Ag were evaluated with AB 1 dye under the UV–visible irradiation for 80 min and the degradation percentages of dye were 10.0, 11.5, 18.8, and 15.9%, respectively. The 3% Ag/TiO_2 film performed the best. An optimal Ag content is required in TiO_2. For the study of the deposition temperature on photodegradation of dye, the percentages were 18.8, 16.7, and 12.8% for films grown at 25, 200, and 400 °C, respectively. 3% Ag/TiO_2 films grown at 200 and 400 °C, intending to enhance the formation of the anatase phase of TiO_2 at the initial design, had become worse in photodegradation of dye as the Ag aggregates became bigger (Fig. 2c and d). These tests confirm the Ag aggregate-free Ag/TiO_2 composite films can have better photocatalytic response. With these screen tests, the photodegradation together with SEM images, we can select the better specimens for antibacterial tests instead of testing all the samples.

3.2. Characterizations of Ag/TiO_2 films after post treatments

For TiO_2 with better crystallinity to further improve its photocatalysis, the 25 °C-deposited Ag/TiO_2 films had undergone different heat treatments. As Ag metal needs to avoid its oxidation and TiO_2 prefers annealing in air to avoid reduction, annealing treatments in inert atmosphere and in air followed by vacuum reduction were tested. Fig. 1c shows the 25 °C-deposited 3% Ag/TiO_2 films after annealing at 600 °C in air with and without the reduction by $NaBH_4$. The 600 °C-air annealed film with and without reduction remained amorphous and its crystallization was difficult. Fig. 3 shows SEM surface images of the 25 °C-deposited 3% Ag/TiO_2 composite films (a) after 600 °C annealing in pure N_2 and (b) after 600 °C annealing in air and a following vacuum reduction at 400 °C. The film annealed at the N_2 atmosphere had Ag precipitates of ~60 nm and was not recommended. The 600 °C-annealed film remained smooth without Ag precipitates and degraded 5.6% dye by photocatalysis. The air-annealed film was reduced in vacuum and degraded 7.1% dye. The vacuum reduction can improve slightly the photocatalysis of Ag/TiO_2.

Fig. 4 shows SEM surface images of the 25 °C-deposited 3% Ag/TiO_2 films after annealing at (a) 400 °C, (b) 500 °C, and (c) 600 °C in air and a following reduction reaction by $NaBH_4$ and (d) SEM image of 25 °C-deposited 3% Ag/TiO_2 film after annealing at 500 °C in air without a reduction reaction for the comparison purpose. Comparing Fig. 4b and d, the oxidized film (Fig. 4d) was clean and the oxidized and reduced film (Fig. 4b) became rough with

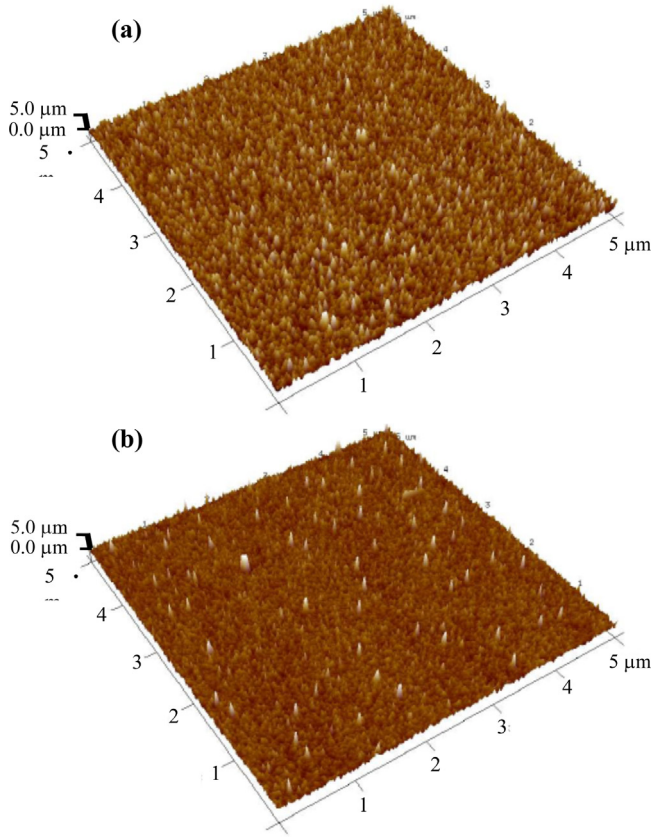

Fig. 5. AFM topographic images of the 25 °C-deposited 3% Ag/TiO_2 films (a) without a post-treatment and (b) after 500 °C annealing in air and a following reduction reaction by $NaBH_4$.

the protrusion of reduced Ag. The Ag protrusion was also clear from Fig. 4a. After air annealing at 600 °C and $NaBH_4$ reduction, the Ag/TiO_2 film had a totally different surface morphology with larger grains. Comparing with Fig. 3(b), the grains after the $NaBH_4$ reduction (Fig. 4c) became much clearer. For the dye degradation tests, the photodegradation percentages were 10.9, 17.7, and 15.9% for films air annealed at 400, 500, and 600 °C, respectively, followed by the $NaBH_4$ reduction. The best photocatalytic performance was for the 3% Ag/TiO_2 film after 500 °C annealing air and a reduction by $NaBH_4$, which was comparable to that of the as-deposited 3% Ag/TiO_2 film. At this stage, we can confirm that the annealing temperature is good at 500 °C and the reduction of 3% Ag/TiO_2 by $NaBH_4$ is much effective to enhance its photocatalysis.

Fig. 5 shows AFM topographic images of the 25 °C-deposited 3% Ag/TiO_2 films (a) without a post-treatment and (b) after 500 °C annealing in air and a following reduction reaction by $NaBH_4$. These two films had shown the comparable photocatalytic capability, 18.8% vs. 17.7%. The images in Figs. 2 b and 4 b were difficult to tell their differences. From AFM surface topographic images, the only difference is that the 500 °C annealed and $NaBH_4$-reduced film has shown a few Ag precipitates.

3.3. Antibacterial performance of Ag/TiO_2 films

Fig. 6 shows survival percentage of *E. coli* bacteria on the bare glass substrate, on the pure TiO_2 film, on the 25 °C-coated Ag/TiO_2 composite films with the Ag contents of 1, 3, and 5%, and on the 25 °C-coated 3% Ag/TiO_2 films annealed at 500 °C in air w/o a following reduction reaction by $NaBH_4$, tested under (a) the dark condition and (b) the illuminated conditions by a 20 W fluorescent lamp illuminated for 30 and 60 min. For soda-lime glass substrate and the pure TiO_2 film, both had increased bacteria amounts after staying a longer period in the dark. Under fluorescent light irradiation, the pure TiO_2 film with BS% (BC%) of 96% (4%) was not effective in bactericide. It looks consistent for pure TiO_2 not as a fluorescent light photocatalyst. For the 25 °C-deposited 1, 3, and 5% Ag/TiO_2 films, they showed the decreased BS% of 91, 68, and 61%, respectively, in the dark due to the increased Ag nanoparticles. After illuminated for 30 min, the 1, 3, and 5% Ag/TiO_2 films had the BS% (BC%) of 81 (19), 5 (95), and 0 (100)%, respectively. BS% (BC%) improved to 59 (41), 0 (100), and 0 (100)% after illuminated for 60 min. After comparing Fig. 6a and b, the 3 and 5% Ag/TiO_2 films displayed the fluorescent light-induced bactericidal performance. Pure TiO_2 film almost did not have the fluorescent light-induced bactericide ability. 3% Ag in TiO_2 is sufficient for bactericide. Ag incorporation in TiO_2 is important to enhance the fluorescent light-induced antibacterial activity. For the 3% Ag/TiO_2 film after 500 °C air annealing, it had BS% of 92 and 73% in the dark and under illumination, respectively. For the 3% Ag/TiO_2 film after 500 °C air annealing and a reduction reaction by $NaBH_4$, its BS% values were 77 and 47% in the dark and under illumination, respectively. From the dye photodegradation, the 25 °C-deposited 3% Ag/TiO_2 film had comparable performance to its film after annealed at 500 °C in air followed by a reduction by $NaBH_4$. However, their bactericidal performance is largely different. The 3 and 5% Ag/TiO_2 films deposited by single-target sputtering can perform the excellent bactericidal performance if they do not undergo the post treatments.

To have a better look of the bactericidal performance, optical photographs of re-cultivated *E. coli* colonies on agar are shown in Fig. 7 for antibacterial tests of pure TiO_2 and 1%, 3%, and 5% Ag/TiO_2 films without and after illumination by a fluorescent lamp for 60 min. Combing with the data in Fig. 6, it can be seen that 3% and 5% Ag/TiO_2 films can largely reduce the bacterial proliferation. No bacteria can survive. However, the 1% Ag/TiO_2 film apparently has a much weak bactericidal ability. Sufficient Ag nano particles in TiO_2 films are required to uniformly decorate the TiO_2 for enhancing antibacterial effect.

There are limited reports for Ag/TiO_2 films with the fluorescent light-induced antibacterial activity. Ogorevc et al. demonstrated the bacteria-killing abilities of 100% for 1% Au-TiO_2 film, 50% for 1% Ag-TiO_2 film, and 0% for pure TiO_2 film under two 15 watt Osram lamps for 90 min illumination [21]. Their films were all prepared by the sol-gel method with the addition of the triblock copolymer of Pluronic F127 into the Ti-containing sol for porosity. Their 1% Ag–TiO_2 film was porous and not optically transparent, and had the antibacterial performance close to ours (1% Ag/TiO_2 shown in Fig. 6b). The consistency in antibacterial activity explains the reliability of our data. For other reports with the antibacterial activity, they had their Ag coated on TiO_2 instead of embedding into TiO_2 films or the Ag aggregated particles in TiO_2 films [22–24]. The bactericidal ability of Ag/TiO_2 films had been attributed to the Ag contribution without the need of light illumination [25–30] or to the photocatalysis under the UV irradiation [31–33]. Few reports can demonstrate the bactericidal photocatalyst films under the indoor lighting with a fast reaction rate [28]. There are also no reports to demonstrate the optical transmittance above 70% for the indoor lighting-induced bactericidal films, with a potential application on window glass. One of the key differences is the Ag aggregation, which has frequently occurred for the sol-gel method [33] and reactive co-sputtering [26,19] w/o a subsequent annealing treatment. The other key difference is the state of TiO_2. Our Ag/TiO_2 was amorphous and did not show the grains and grain boundaries, while other works had attempted to anneal for crystallization. There is another promising system of the CNT-added TiO_2 films to show the excellent visible light photo-inactivation, but it needs 20 wt% CNT [34].

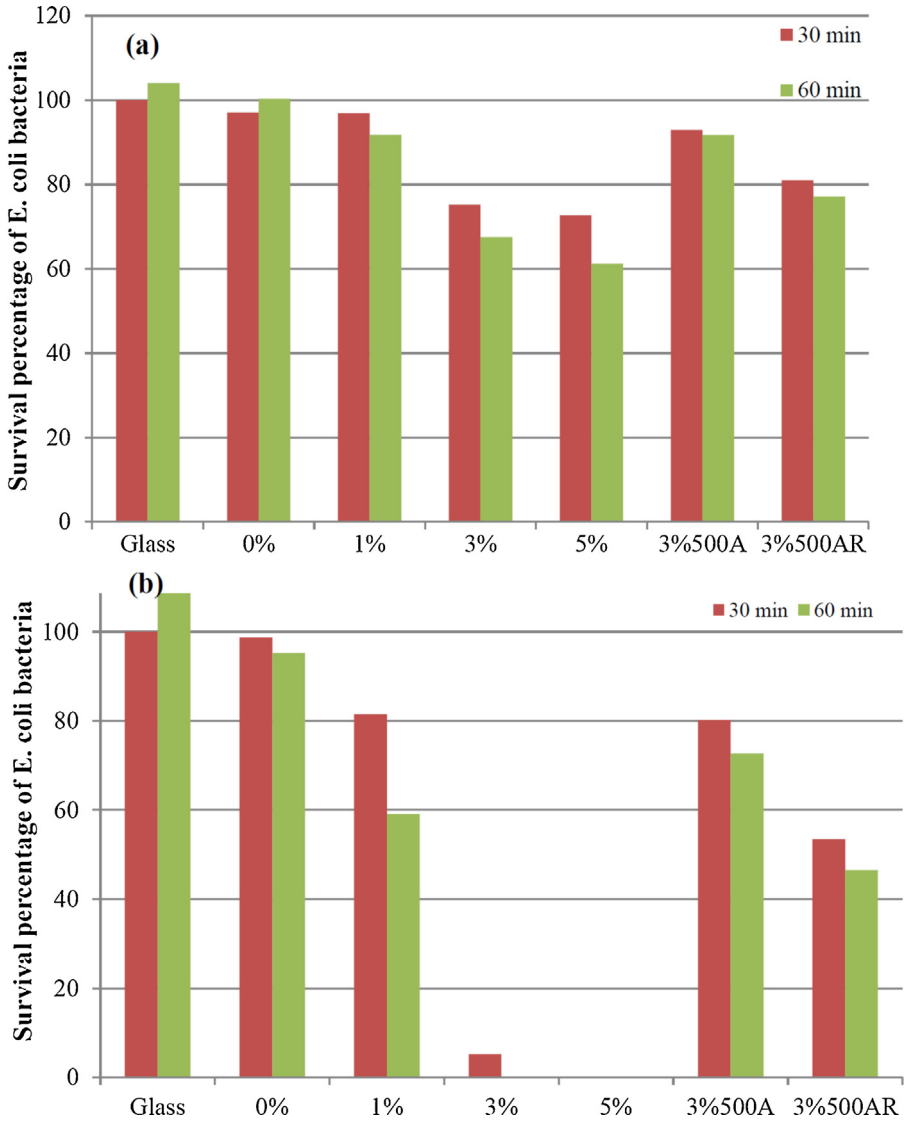

Fig. 6. Survival percentage of *E. coli* bacteria on the bare glass substrate, on the pure TiO_2 film, on the 25 °C-coated Ag/TiO_2 composite films with the Ag contents of 1, 3, and 5%, and on the 25 °C-coated 3% Ag/TiO_2 films annealed at 500 °C in air (A) w/o a following reduction reaction by $NaBH_4$ (R), tested under (a) the dark condition and (b) the illuminated conditions by a 20 W fluorescent lamp illuminated for 30 and 60 min.

3.4. Exploring the fluorescent light-induced antibactericidal mechanism

To elucidate the excellent performance, the 25 °C-deposited 3% Ag/TiO_2 film was evaluated by TEM. Fig. 8 shows (a) low and (b) high magnified TEM images of the 3% Ag/TiO_2 composite films without post treatments. From the cross-sectional image, the film had a thickness of 80 nm. The Ag nanoparticles in film were smaller than 8 nm and they were uniformly distributed except the clustering close to the glass substrate. The Ag nanoparticle was crystallized and identified by the lattice fringe in Fig. 8b. However, the TiO_2 matrix could not obtain the diffraction spots and remained amorphous with a disordered microstructure. The amorphous nature from the TEM test is consistent with the result shown in Fig. 1(b). This TEM analysis declares that it is no need for TiO_2 in Ag/TiO_2 films to be well crystallized or to be an anatase phase for better indoor light antibacterial activity.

Fig. 9 shows optical transmittance of the 25 °C-deposited TiO_2, 3% Ag/TiO_2, 5% Ag/TiO_2 composite films, and the 25 °C-deposited 3% Ag/TiO_2 films annealed at 500 °C in air without and with a following reduction reaction by $NaBH_4$. The pure TiO_2, 3% Ag/TiO_2, and 5% Ag/TiO_2 films had the transmittance above 75, 70, and 65%, respectively, in the range of 300–800 nm. Both of the air annealed films without and with the $NaBH_4$ reduction had the exactly same transmittance above 70% across the whole wavelength range of 300–800 nm except a deep absorption at 400 nm. The deep absorption at 400 nm has been frequently observed for the photocatalysts with Ag nanoparticles to enhance the visible light absorption by the surface plasmonic resonance. Together with the microstructural analysis, both of the 500 °C air-annealed Ag/TiO_2 films without (Fig. 4d) and with (Figs. 4 b and 5 b) the $NaBH_4$ reduction all behaved the same with a small amount of Ag precipitation to contribute to the 400 nm absorption.

The 25 °C-deposited 3% Ag/TiO_2 film with a smooth surface, a uniform distribution of Ag nanoparticles ≤ 8 nm in size, an indoor light-induced bactericidal ability under a weak 20 W fluorescent lamp, and an optical transmittance >70% in the wavelength range of 300–800 nm is promising to be used as a transparent window coating and coatings for living environment and public facilities, where the weak indoor lighting is sufficient for the photocatalytic bactericide.

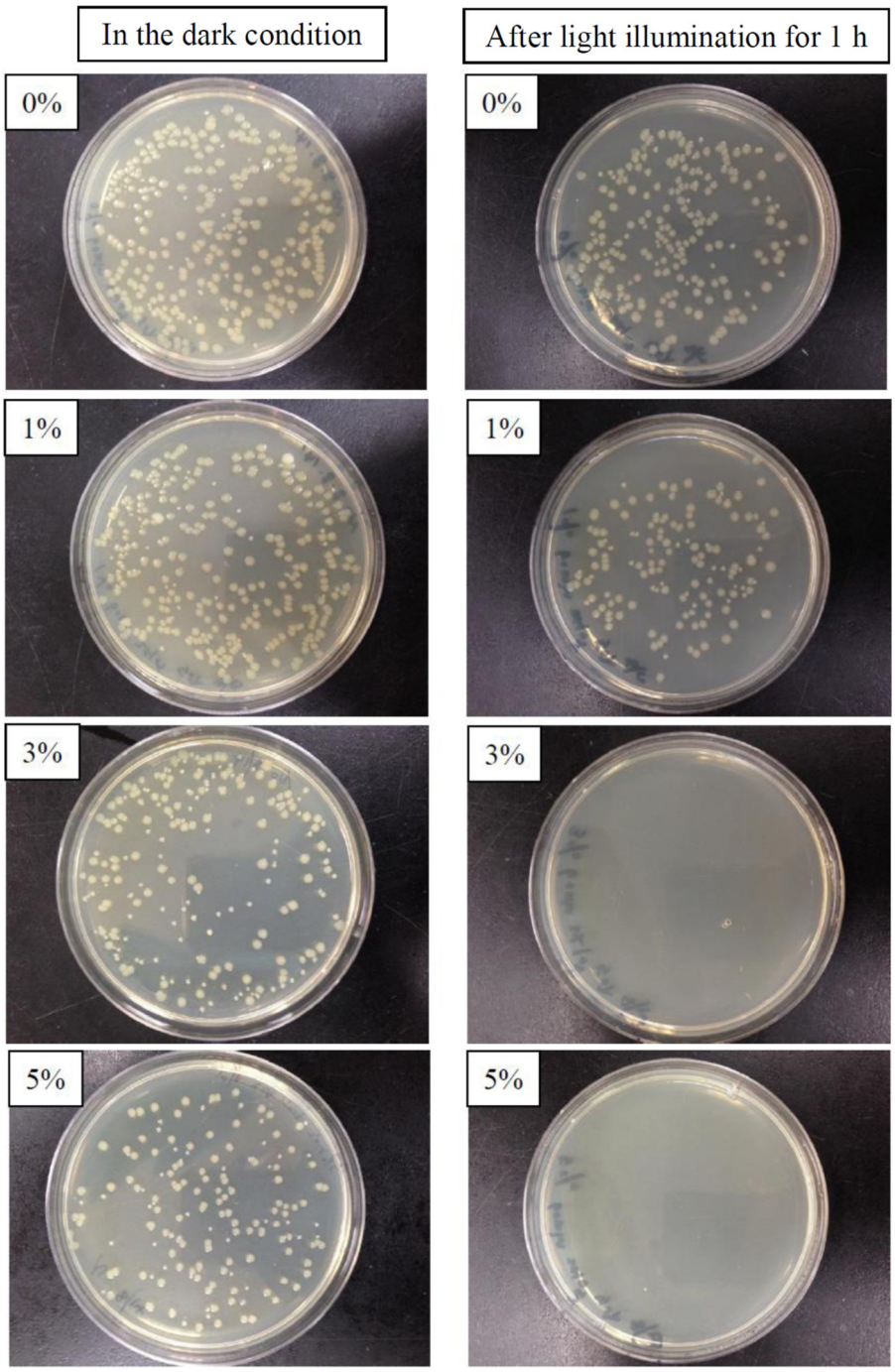

Fig. 7. Typical optical photographs of re-cultivated *E. coli* colonies on agar for antibacterial tests of pure TiO_2 and 1%, 3%, and 5% Ag/TiO_2 films without and after illumination by a fluorescent lamp for 60 min.

There are three issues arise from this study. Firstly, how can this Ag/TiO_2 film be fluorescent light excited for bactericide, while it is not for pure TiO_2 film with the same behavior in optical transmittance? Secondly, what is the mechanism for the indoor light-induced antibacterial activity? Thirdly, why have other similar works not observed the indoor light photocatalytic bactericide? Based upon Fig. 9b, Plots of $(\alpha h\nu)^2$ vs. photon energy $(h\nu)$ for the optical band gap determination, we could calculate the direct energy band gap by using the Tauc equation [35].

$$(\alpha h\nu)^2 = A(h\nu - E_g)$$

where α is absorption coefficient, A is a constant, $h\upsilon$ is the incident photon energy, and E_g is the energy band gap of the test films. The E_g values were 3.67, 3.67, and 3.70 eV for pure TiO_2 and 3% and 5% Ag/TiO_2, respectively. The amorphous TiO_2-based films had much high E_g values than the expected 3.2–3.4 eV for TiO_2. The annealed and the annealed plus reduction films had an absorption peak for band gap of 2.79 eV, because of the surface plasmonic resonance of precipitated Ag nanoparticles. Therefore, our 3% Ag/TiO_2 film with good bactericidal performance cannot be excited by the fluorescent lamp with the light wavelength between 380–780 nm. The existing electrons and holes come from thermal equilibrium and their numbers are low at room temperature. For the specimens

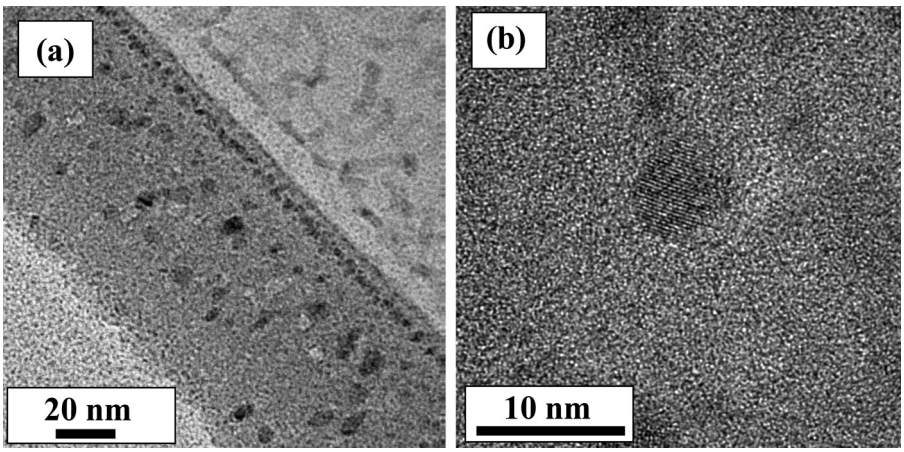

Fig. 8. (a) Low and (b) high magnified TEM images of the 25 °C-deposited 3% Ag/TiO_2 composite films without a following annealing procedure.

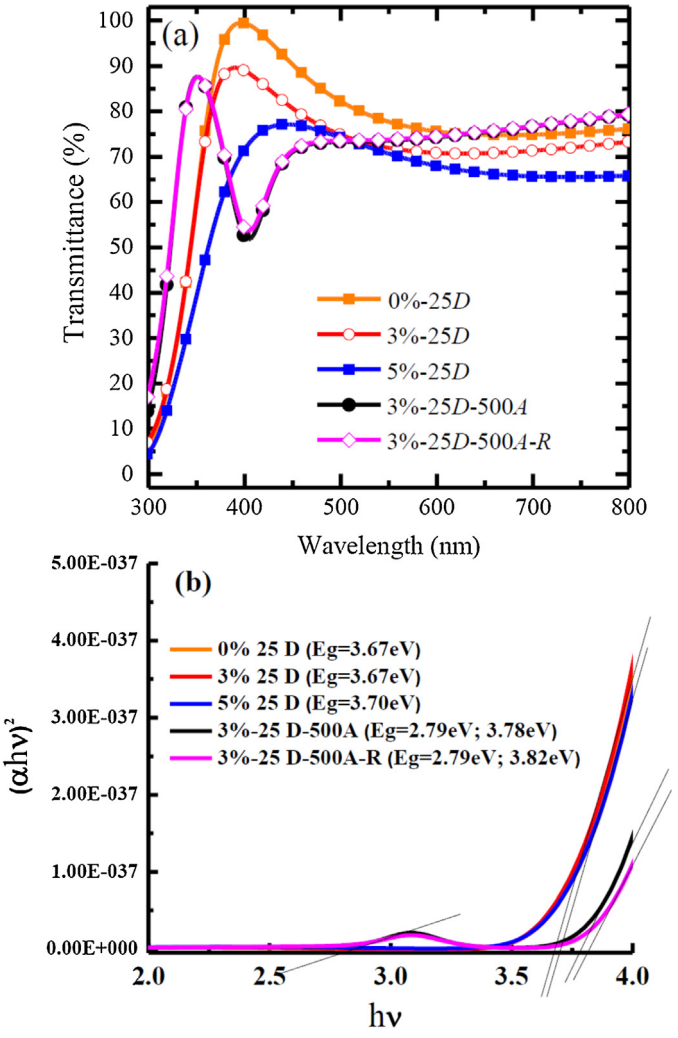

Fig. 9. (a) Optical transmittance and (b) Plots of $(\alpha h\nu)^2$ vs. photon energy ($h\nu$) for the optical band gap determination of the 25 °C-deposited TiO_2, 3% Ag/TiO_2, and 5% Ag/TiO_2 films and the 25 °C-deposited 3% Ag/TiO_2 films annealed at 500 °C in air (A) without and with a following reduction reaction by $NaBH_4$ (R).

with the SPR effect, their bactericidal effect is not good. As pure TiO_2 does not show the same bactericidal behavior, the incorporation of the dispersed Ag nanoparticles into TiO_2 is the key point. As pure TiO_2 alone is not useful and the Ag nanoparticles in TiO_2 (Fig. 8) are not covering the whole film surface, the antibacterial ability of 3% Ag/TiO_2 film comes from the synergy effect of TiO_2 and Ag nanoparticles. To form the dispersed Ag in Ag/TiO_2, the first thing to note, based upon our processing and experimental data, is the Ag added to target needs to be in nanometer size through a chemical route instead of physical mixing of powders for uniform separation. The second one is the Ag in Ag/TiO_2 films cannot come from the co-sputtering of a pure Ag target and a Ti target, because the Ag atom flow coming out from the same target has the great chance to form aggregates. The third one is that high temperature processes, e.g., gas phase deposition and sol–gel chemical process, for the Ag/TiO_2 system have a chance for the Ag aggregation. The well-dispersed Ag nanoparticle has the major role to effectively separate the electrons and holes by attracting the electron to prolong the lifetime of holes for bactericide. The electron and hole pairs in the TiO_2 matrix of Ag/TiO_2 are not generated from the fluorescent light-induced excitation due to its large band gap of 3.67 eV, but from the thermal equilibrium. Under the dark condition, the charge carriers at its thermal equilibrium are few in quantity for antibacterial activity and they also have a short lifetime leading to the fast charge recombination. For Ag/TiO_2 without the indoor light irradiation (Fig. 6a), its thermally induced charge carriers are few and it becomes holes dominant after the electrons are trapped by Ag nanoparticles. These holes with a low migration velocity will have a small travel area or hole-affecting zone to interact with microbes. Under the indoor light lighting, the thermal charge carriers on Ag/TiO_2 can be accelerated by the driving force of electrical field of light to have a higher drift velocity, to assist the charge separation through the electron attraction by Ag nanoparticles, and to achieve the larger hole-affecting zone. Those microbes located in the hole-affecting zone will undergo the bactericidal reaction after they react with •OH radicals and H_2O_2, which come from the hole reaction with H_2O.

Fig. 10 shows the bactericide mechanism of the 3% Ag/TiO_2 films under the illumination of a fluorescent lamp. To differentiate the bactericidal effect, pure TiO_2 (a,b) and 3% Ag//TiO_2 films (c,d) are tested without the illumination and under a fluorescent lamp. In this model, the electrons and holes at thermal equilibrium are co-existing in TiO_2 films and quickly recombine together. In 3% Ag–TiO_2 film, the total net charge carrier is electronic holes. These holes have a small affecting zone due to the nature of their random-walk propagation. However, the hole affecting zone become larger ($\lambda_2 > \lambda_1$) due to the drift nature under the electric field of the fluorescent light. Other factors to affect the size of the hole-affecting zone include the charge concentration of TiO_2, point defect, line defect, plane defect, crystallinity of TiO_2, second phases, surface

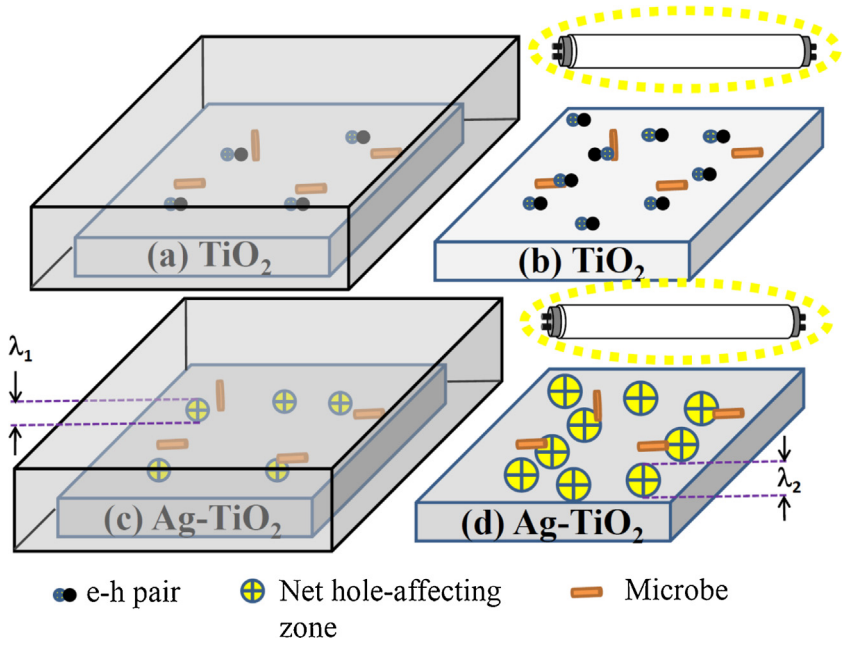

Fig. 10. Bactericide mechanism of the 3% Ag/TiO_2 films under the illumination of a fluorescent lamp. To differentiate the bactericidal effect, pure TiO_2 (a,b) and 3% Ag//TiO_2 films (c,d) are tested without the illumination and under a fluorescent lamp.

state etc. The larger the hole-affecting zone, the easier for the bactericide. For our case of 3% Ag/TiO_2 film, the hole propagation is accelerated by electric field and does not hinder by the glassy sate. During its propagation, the low carrier concentration at thermal equilibrium in TiO_2, caused by its high E_g of 3.67 eV, lower its interference with other charges to lengthen its mean free path.

The bactericidal performance of our work cannot be totally attributed to the Ag^+ leaching at this stage. If the leaching Ag^+ is the only bactericidal medium [28,29,36], both of the bactericidal experiments in the dark room and under the illumination of a fluorescent lamp should have the same performance. In the dark condition, the 3% Ag/TiO_2 and 5% Ag/TiO_2 films had the bacteria-killing abilities or BC% of 30% and 40% (Fig. 6a), respectively. Under the indoor lighting, they reached 100% bacteria killing. It is expected that the higher Ag content and the wide Ag affecting zone can finally reach the 100% bacteria killing in the dark without the need of lighting. However, the many Ag nanoparticles in TiO_2 for 100% bacteria killing can lead to another environmental risk in the peeling of Ag nanoparticles. Our 3% Ag/TiO_2 film can be viewed as the film with the extremely low Ag content for the environmental sake.

At last, we need to firstly emphasize that Ag is good at bactericide but too many Ag contents or Ag aggregates will lead to low optical transmittance and no visible light-induced bactericide. Here the non-aggregated Ag nanoparticle had the particle size less than 8 nm. The Ag aggregates in Figs. 2 and 3 have the size of 20–40 nm, which had been also mentioned as Ag nanoparticle. The limited bactericide ability for Ag/TiO_2 composite films with bigger Ag aggregates is mainly contributed from the Ag aggregates itself. Secondly, our TiO_2 in good 3% Ag/TiO_2 films is amorphous instead of trying to form the anatase phase by substrate heating or annealing.

4. Conclusions

Transparent Ag/TiO_2 composite films with the Ag contents of 0, 1, 3, and 5 vol.% were successfully deposited at 25, 200, and 400 °C on glass substrates by radio frequency sputtering with a single cermet target formed by hot pressing the Ag nanoparticle-decorated TiO_2 powder. The as-deposited films and films after post treatments by annealing and/or reduction were evaluated for their crystal structure, microstructure, photodegradation ability in dye, optical property, and bactericide ability with and without fluorescent lamp lighting. The 25 °C-deposited 3% Ag/TiO_2 film with smooth morphology and an amorphous structure had performed the best in dye degradation and in the fluorescent light-induced bactericide ability. Any high temperature post treatment that caused the Ag oxidation or Ag protrusion due to aggregation had led to the worse and ineffective photocatalysis. The reason of the fluorescent light-induced bactericide ability for the 3% Ag/TiO_2 film is related to the synergy effect of the uniformly distributed Ag nanoparticles in TiO_2, the enhanced drift velocity of thermally induced charge carriers under the assistance of the electrical field from the fluorescent lamp lighting, and the low charge carrier to avoid the interference of the hole propagation in the amorphous TiO_2 with higher band gap of 3.67 eV than the annealed one at 2.79 eV. The bactericide mechanism based upon the size change of the hole-affecting zone with the process condition is proposed. The Ag^+ release mechanism is not a major factor. The transparency above 70% is attributed to the uniform distribution and small quantity of the Ag nanoparticles. Our thin Ag/TiO_2 film with the indoor lighting-induced bactericide ability and the photodegradation ability in dye can provide the environmental protections by applying to the private and public facilities.

Acknowledgements

This work was supported by Ministry of Science and Technology of the Republic of China under grant numbers MOST 103-2218-E-011-015 and MOST 104-2218-E-035-004 and by the National Taiwan University of Science and Technology through grant number 103H451201.

References

[1] A. Fujishima, K. Honda, Nature (London) 238 (1972) 37–38.
[2] S.A. Tomás, S. Stolik, R. Palomino, R. Lozada, C. Persson, I. Pepe, A. Ferreira da Silva, J. Appl. Phys. 98 (2005) 073516.
[3] I. Hayakawa, Y. Iwamoto, K. Kikuta, S. Hirano, Sens. Actuators B 62 (2000) 55–60.

[4] L.Z. Zhang, J.C. Yu, H.Y. Yip, Q. Li, K.W. Kwong, A.W. Xu, P.K. Wong, Langmuir 19 (2003) 10372–10380.
[5] Z.G. Xiong, J.Z. Ma, W.J. Ng, T.D. Waite, X.S. Zhao, Water Res. 45 (2011) 2095–2103.
[6] A.L. Linsebigler, G. Lu, J.T. Yates Jr., Chem. Rev. 95 (1995) 735–758.
[7] S. Ito, T. Takeuchi, T. Katayama, M. Sugiyama, M. Matsuda, T. Kitamura, Y. Wada, S. Yanagida, Chem. Mater. 15 (2003) 2824–2828.
[8] S. Girish Kumar, L. Gomathi Devi, J. Phys. Chem. A 115 (2011) 13211–13241.
[9] Y. Wang, Q. Wang, X. Zhan, F. Wang, M. Safdar, J. He, Nanoscale 5 (2013) 8326–8339.
[10] A. Takai, P.V. Kamat, ACS Nano 5 (2011) 7369–7376.
[11] P.V. Kamat, J. Phys. Chem. C 111 (2007) 2834–2860.
[12] W. Hou, S.B. Cronin, Adv. Funct. Mater. 23 (2013) 1612–1619.
[13] J. Choi, H. Park, M.R. Hoffmann, J. Phys. Chem. C 114 (2010) 783–792.
[14] I.M. Arabatzis, T. Stergiopoulos, M.C. Bernard, D. Labou, S.G. Neophytides, P. Falaras, Appl. Catal. B–Environ. 42 (2003) 187–201.
[15] E.S. Bardos, H. Czili, A. Horvath, J. Photochem. Photobiol. A: Chem. 154 (2003) 195–201.
[16] K. Naoi, Y. Ohko, T. Tatsuma, J. Am. Chem. Soc. 126 (2004) 3664–3668.
[17] L.L. Bao, S.M. Mahurin, S. Dai, Anal. Chem. 76 (2004) 4531–4536.
[18] L. Armelao, D. Barreca, G. Bottaro, A. Gasparotto, C. Maccato, E. Tondello, O.I. Lebedev, S. Turner, G. Van Tendeloo, C. Sada, U.L. Stangar, ChemPhysChem 10 (2009) 3249–3259.
[19] J. Okumu, C. Dahmen, A.N. Sprafke, M. Luysberg, G. von Plessen, M. Wuttig, J. Appl. Phys. 97 (2005) 094305.
[20] J. Zuo, P. Keil, G. Grundmeier, Appl. Surf. Sci. 258 (2012) 7231–7237.
[21] J.Ŝ. Ogorevc, E.T. Pirc, L. Matoh, P. Bukovec, Acta Chim. Slov. 59 (2012) 264–272.
[22] M.S. Wong, D.S. Sun, H.H. Chang, PloS One 5 (2010) e10394.
[23] J. Li, Y. Qiao, H. Zhu, F. Meng, X. Liu, Intl. J. Nanomed. 9 (2014) 3389–3402.
[24] J. Mungkalasiri, L. Bedel, F. Emieux, J. Doré, F.N.R. Renaud, C. Sarantopoulos, F. Maury, Chem. Vap. Depos. 16 (2010) 35–41.
[25] J. Li, X. Liu, Y. Qiao, H. Zhu, C. Ding, Colloid Surf. B-Biointerfaces 113 (1341) (2014) 23.
[26] P. Navabpour, S. Ostovarpour, J. Hampshire, P. Kelly, J. Verran, K. Cooke, Thin Solid Films 571 (2014) 75–83.
[27] J. Li, Y. Qiao, H. Zhu, F. Meng, X. Liu, Int. J. Nanomed. 9 (2014) 3389–3402.
[28] O. Akhavan, J. Colloid Interface Sci. 336 (2009) 117–124.
[29] K. Jamuna-Thevi, S.A. Bakar, S. Ibrahim, N. Shahab, M.R.M. Toff, Vacuum 86 (2011) 235–241.
[30] B.S. Necula, J.P.T.M. van Leeuwen, L.E. Fratila-Apachitei, S.A.J. Zaat, I. Apachitei, J. Duszczyk, Acta Biomater. 8 (2012) 4191–4197.
[31] B. Xi, X. Chu, J. Hu, C.S. Bhatia, A.J. Danner, H. Yang, Appl. Surf. Sci. 311 (2014) 582–592.
[32] K. Mao, Y. Li, H. Zhang, W. Zhang, W. Yan, Clean-Soil, Air Water 41 (2013) 455–462.
[33] B. Yu, K.M. Leung, Q. Guo, W.M. Lau, J. Yang, Nanotechnology 22 (2011) 115603.
[34] O. Akhavan, R. Azimirad, S. Safa, M.M. Larijani, J. Mater. Chem. 20 (2010) 7386–7392.
[35] S. Muthukumaran, R. Gopalakrishnan, Opt. Mater. 34 (2012) 1946–1953.
[36] S.H. Uhm, D.H. Song, J.S. Kwon, S.B. Lee, J.G. Han, K.N. Kim, J. Biomed. Mater. Res. Part B 102 (2014) 592–603.